1	Carbonaceous microstructures from sedimentary laminated chert within the					
2	3.46 Ga Apex Basalt, Chinaman Creek locality, Pilbara, Western Australia					
3						
4	Keyron Hickman-Lewis ^{a*} , Russell J. Garwood ^b , Martin D. Brasier ^{c+} , Tomasz Goral ^d ,					
5	Haibo Jiang ^e , Nicola McLoughlin ^f and David Wacey ^{g,h*}					
6						
7	^a St Edmund Hall, Queens Lane, Oxford, OX1 4AR, United Kingdom and Department					
8	of Earth Sciences, South Parks Road, Oxford, OX1 3AN, United Kingdom. Present					
9	Address: "Homestead", 19 Sunnybank Road, Blackwood, Gwent, NP12 1HT					
10	^b School of Earth, Atmospheric and Environmental Sciences, The University of					
11	Manchester, Manchester, M13 9PL, United Kingdom					
12	^c Department of Earth Sciences, South Parks Road, Oxford, OX1 3AN, United					
13	Kingdom					
14	^d Imaging and Analysis Centre, Natural History Museum, Cromwell Road, South					
15	Kensington, London, SW7 5BD, United Kingdom					
16	^e Department of Materials, Parks Road, Oxford, OX1 3PH, United Kingdom					
17	^f Department of Earth Sciences and Centre for Geobiology, University of Bergen,					
18	Allegaten 41, N-5007 Bergen, Norway					
19	^g School of Earth Sciences, Life Sciences Building, University of Bristol, 24 Tyndall					
20	Avenue, Bristol, BS8 1TH, United Kingdom					
21	^h Centre for Microscopy Characterisation and Analysis, and Centre of Excellence for					
22	Core to Crust Fluid Systems, The University of Western Australia, 35 Stirling					
23	Highway, Perth, WA 6009, Australia					
24						

25 † Deceased

26 *To whom correspondence should be addressed.

27 E-mail: Hickman.Lewis@gmail.com or David.Wacey@uwa.edu.au

28

29 Abstract

Hydrothermal black chert veins intruding the 3.46 Ga Apex Basalt contain some of
Earth's oldest microfossil-like objects, whose biogenicity has been questioned. Whilst
these black chert veins have been studied in great detail, relatively little is known
about the stratiform, seafloor, sedimentary cherts that are conformably interbedded
with volcanic rocks of the Apex Basalt.

35

36 Herein, we document and assess the biogenicity of carbonaceous microstructures 37 present in the lowermost of the stratiform chert units (informally known as the 'Apex 38 chert'), at the Chinaman Creek locality in the Marble Bar greenstone belt, Pilbara 39 Craton, Western Australia. Carbonaceous material mostly occurs within clotted grey-40 black cherts and microgranular 'grainstone-like' cherts within the stratiform unit, the 41 latter being the major focus of this study. In the clotted cherts, carbon occurs as 42 lobate, fluffy grains, rare compressed flakes, and as a grain boundary phase around 43 spherulitic silica. There is no morphological evidence to support the biogenicity of 44 these microstructures. In contrast, the microgranular chert contains fluffy and flaky 45 carbonaceous grains, plus laminated grains comprising multiple non-isopachous 46 wrinkled carbonaceous laminae, with noted thickening towards some ridge crests, as 47 determined by confocal laser scanning microscopy. Roll-up structures provide 48 evidence of an initial plasticity, interpreted to have formed via the tearing-up and 49 current-induced plastic deformation of microbial mat fragments. Geochemical 50 mapping, using laser Raman micro-spectroscopy and NanoSIMS, respectively

51	demonstrates the antiquity of the carbon, and reveals a close correlation between						
52	carbon, nitrogen and sometimes sulfur, concentrated within dark brown to black						
53	laminae. Adjacent to microgranular zones are zones of more persistent carbonaceous,						
54	undulose, filament-like laminae that entrain relict sediment grains. These						
55	microstructures are directly comparable to a sub-type of microbially induced						
56	sedimentary structure (MISS), widely reported from younger siliciclastic sediments						
57	colonized by microbial biofilms.						
58							
59	The morphology and chemical composition of both the non-isopachous laminated						
60	grains and the filament-like laminae are consistent with a biological interpretation,						
61	suggesting microscopic MISS were present in the microgranular stratiform 'Apex						
62	chert'. However, the fact that neither macroscopic MISS nor bona fide microfossils						
63	have yet been reported from this unit, coupled with the proximity of these structures						
64	to active hydrothermal vents, potentially discharging hot carbon-rich fluids, urges						
65	caution in such an interpretation. The Chinaman Creek 'Apex chert' investigated here						
66	is one of at least five sedimentary, laminated cherts within the Apex Basalt. These						
67	horizons are promising targets in the search for biological activity within a						
68	dominantly volcanic Archean environment.						
69							
70	Keywords: Apex chert; Pilbara; Carbon; MISS; Archean life						
71							
72	1. Introduction						
73	The 3.46 Ga Apex Basalt in the Marble Bar greenstone belt of the Pilbara Craton,						

74 Western Australia, has long been a focus for the investigation of early Earth

environments and potential microbial life. It is particularly notable for the presence of

76 carbonaceous filamentous microstructures in hydrothermal black chert veins at the 77 Chinaman Creek locality, interpreted as representing eleven species of fossilized 78 prokaryotes (Schopf and Packer, 1987; Schopf, 1992, 1993, 1999). However, the 79 biogenicity of these 'microfossils' has been highly debated (e.g., Brasier et al., 2002, 80 2005, 2011; Schopf et al., 2002, 2007, 2010; Schopf and Kudryavtsev, 2009, 2012, 81 2013; Marshall et al., 2011; Ollcott Marshall and Marshall, 2013). Recent 82 morphological and geochemical analyses at a high spatial resolution have shown the 83 filaments to be mineral artifacts comprising chains of phyllosilicate crystals that later 84 adsorbed carbon during fluid flow within an active hydrothermal system (Brasier et 85 al., 2015; Wacey et al., 2015), or carbon-filled cracks (Bower et al., 2016). Biogenic 86 stromatolitic clasts have also been postulated in the Apex hydrothermal chert veins 87 (Schopf, 1993), though these were subsequently reappraised as isopachous, abiogenic, 88 stromatoloidal internal cements, occurring in a later stage chert fabric (fabric B2 of 89 Brasier et al., 2005).

90

91 Despite the controversy over the presence of life in the Apex hydrothermal chert 92 veins, the Apex Basalt remains a promising rock unit to investigate early life on Earth. 93 It is well-preserved, having undergone metamorphism to no greater extent than 94 prehnite-pumpellyite to lower greenschist facies (Hickman and Lipple, 1978; Van 95 Kranendonk et al., 2007). It also contains at least five stratiform chert units (Kato and 96 Nakamura, 2003; Van Kranendonk, 2006); these are concordant, bedding parallel 97 units that are often internally laminated and preserve sedimentary structures (Kato and 98 Nakamura, 2003; Brasier et al., 2011). Hence, these may provide evidence of 99 sedimentary environments (and their associated biotas) reflecting quiescent periods in 100 an otherwise volcanic 'Apex time'. In some recent studies it has proven effective to

- 101 look in volcanically influenced terranes for signs of early life (e.g., Walsh, 2004;
- 102 Westall et al., 2006, 2015), since these provide many of the minor elements essential

103 for life (e.g. Cu, Co, Ni and Fe; Barras, 2012). Volcanic lithologies have shown the

- 104 capability to foster modern extremophilic life; shortly following their eruption,
- 105 bacterial communities are able to benefit from the diverse, often metallic, elements
- 106 present (Cockell et al., 2009; Kelly et al., 2011, 2014).
- 107

108 Here, we investigate the lowermost of the stratiform chert horizons of the Apex Basalt

109 at the Chinaman Creek locality (Unit 4 of Brasier et al., 2005, 2011; informally

110 referred to as the 'Apex chert'), outlining the modes of occurrence of carbonaceous

111 material, and assessing the likelihood of a biogenic component. In so doing, we

112 consider that very ancient/alien putative biogenic structures and geochemical signals

should not be accepted as being of biological origin without geologically-plausible

non-biological origins first being tested and falsified (cf. Brasier et al., 2004a).

115

116 **2. Methods**

117 2.1. Field mapping and petrographic analysis

118 Field mapping in the Marble Bar greenstone belt was undertaken by us as part of a 119 wider programme with the Geological Survey of Western Australia, supplemented by 120 a detailed programme of mapping and sampling of the Apex Basalt across an area of 121 around 12 km². Multiple samples were collected from the Chinaman Creek locality 122 between 1999 and 2006, located by means of satellite images and Global Positioning 123 Systems (GPS). For the stratiform 'Apex chert', samples were collected across the full 124 1.5 km of available outcrop, encompassing each of the north, central and south blocks 125 described in Brasier et al. (2005, 2011). Optical petrography and fabric mapping was

performed in the Department of Earth Sciences imaging laboratory, Oxford
University, using standard 30 µm and 100 µm petrographic thin sections. Thin
sections were examined under bright-field, polarized transmitted, and incident
(reflected) light using Nikon Optiophot-2 (biological) and Optiophot-pol (polarizing)
microscopes. Images were obtained using a single-chip CCD camera, providing live
images in full RGB colour, and processed using AcQuis and Auto-Montage image
capturing software.

133

134 2.2. Confocal Laser Scanning Microscopy (CLSM)

135 Confocal images were acquired for numerous features observed in thin-sections using

a Nikon A1-Si laser-scanning confocal microscope using either a 20x or 40x oil-

137 immersion objective (numerical apertures of 0.7 or 1.3, respectively). Images were

recorded with pixel dimensions between 0.31 and 0.61 µm. Autofluorescence of the

specimens was excited with the following laser lines: 405-nm line of 100 mW cube

140 laser (Coherent Inc., USA, http://www.coherent.com), 488-nm line of 50 mW

141 sapphire laser (Coherent Inc., USA), 561-nm line of 50 mW sapphire laser (Coherent

142 Inc., USA) and 640-nm line of 40 mW cube laser (Coherent Inc., USA).

143 Autofluorescence signal was collected with 4 PMT detectors with the following

144 wavelength emission windows: 425–475 nm for the 405 nm laser, 500–550 nm for the

145 488 nm laser, 570–620 nm for the 561 nm laser, and 675–725 nm for the 640 nm

146 laser. The specimens were visualised using a 29.9 μ m (1.2 airy units) confocal

147 pinhole and a number of z-stacks (typically between 10 and 50), of optical thickness

148 between 0.2–2.0 µm each, were acquired. The fluorescence signal from each z-stack

149 was then projected onto a maximum projection image and used to generate a 3D

150 model of the specimen using Nikon NIS-Elements software (www.nis-elements.com)

for Figure 13c. The stacks were further explored and visualised using volume
rendering; they were loaded using the open source software Fiji (Schindelin et al.,
2012), and the channel with maximum contrast converted to a grayscale TIFF. The
resulting TIFF stacks were subsequently loaded in the open source software Drishti
(Limaye, 2012), and volume rendered by modifying the 2D histogram transfer
function. These renders were used as the basis for Figure 13b, d and for
supplementary movie 1.

158

159 2.3. Nano-scale Secondary Ion Mass Spectrometry (NanoSIMS)

160 NanoSIMS was performed in the Department of Materials, University of Oxford,

161 using a CAMECA NanoSIMS 50. Regions of interest (ROI) were identified under the

162 optical microscope in polished 30 µm thin sections, and then micro-mapped using

163 bright-field and reflected light. The reflected light images were subsequently used to

164 locate the surface expressions of laminated features within the NanoSIMS. Discs of c.

165 10 mm diameter containing the ROI were extracted from the thin sections, mounted

166 on NanoSIMS stubs, and coated with a thin (5-10 nm) layer of platinum to provide

167 conductivity at high voltage. Details of qualitative elemental mapping using

168 NanoSIMS in multi-collector mode are given in Wacey et al. (2008) and Kilburn and

169 Wacey (2011). Briefly, a focused primary Cs+ ion beam, with a beam current of 2–4

170 pA, was rastered over the sample surface, and the sputtered ions were extracted to a

171 double focusing mass spectrometer. Images with sub-100 nm spatial resolution

172 mapping relative ion intensity were acquired over fields of view ranging from $10 \ \mu m$

- 173 $\,$ to 25 $\mu m.$ Prior to each analysis, the sample area was pre-sputtered to remove surface
- 174 contamination, implant Cs⁺ ions into the sample matrix and attain an approximate
- 175 steady state of secondary ion emission (cf. Gnaser, 2003). Ion maps of carbon $({}^{12}C)$,

nitrogen (¹²C¹⁴N⁻), silicon (²⁸Si⁻), sulfur (³²S⁻) and phosphate (³¹P¹⁶O₂⁻) were then
produced simultaneously from the same sputtered volumes of sample. Only relative
concentrations of elements can be obtained using this NanoSIMS methodology.
Without multiple standards, no inferences can be made from these data concerning
either the absolute concentration of elements, or the percentage concentration of one
element compared to another.

182

183 2.4. Laser Raman Microspectroscopy

184 Raman was performed in the Centre for Microscopy, Characterisation and Analysis

185 (CMCA), The University of Western Australia, using a WITec alpha 300RA+

186 instrument with a *Toptica Photonics Xtra II* 785 nm laser source. Laser excitation

187 intensity at the sample surface was in the 1-5 mW range, well below the intensity that

188 may damage carbonaceous material (e.g., Everall et al., 1991) and comparable to

189 previous studies of the Apex chert (e.g., Olcott Marshall et al., 2012; Sforna et al.,

190 2014). The laser was focused through either a 20x/0.4 or 100x/0.9 objective, with the

191 latter giving a spot size of smaller than 1 µm. Spectral acquisitions were obtained

192 with 600 l/mm grating and a peltier-cooled (-60 °C) 1024 x 128 pixel CCD detector.

193 Laser centering and spectral calibration were performed daily on a silicon chip with

194 characteristic Si Raman band of 520.4 cm⁻¹. Count rates were optimised prior to point

spectra acquisition or hyperspectral mapping using the dominant quartz Raman band

196 of 465 cm⁻¹. Spectra were collected in the 100-1800 rel. cm⁻¹ region in order that both

197 1st order mineral vibration modes and 1st order carbonaceous vibration modes could

198 be examined simultaneously. Raman maps were acquired with the spectral centre of

199 the detector adjusted to 944 cm⁻¹, with a motorised stage allowing XYZ displacement

200 with precision of better than 1 μ m. Spectral decomposition and subsequent image

201	processing were performed using WITec Project FOUR software, with baseline						
202	subtraction using a 3 rd or 4 th order polynomial. Carbon maps were created by						
203	integrating over the ~1600 cm ⁻¹ 'G' Raman band and quartz maps created by						
204	integrating over the 465 cm ⁻¹ quartz Raman band. The ~1350 cm ⁻¹ carbon 'D' Raman						
205	band was not used to construct maps because this may suffer from interference from						
206	the ~1320 cm ⁻¹ hematite Raman band (cf. Marshall and Olcott Marshall, 2013). Point						
207	spectra were acquired using the 100x/0.9 objective, an integration time of 0.5 s and 10						
208	accumulations. All analyses were conducted on material embedded below the surface						
209	of the thin section to avoid artefacts in the Raman spectra resulting from polishing						
210	and/or surface contamination.						
211							
212	2.5. Energy dispersive elemental mapping (EDS)						
213	Elemental analysis and mapping over several millimeters of Chinaman Creek thin						
214	sections was performed on a FEI Verios 460 SEM equipped with an Oxford						
215	Instruments X-Max 80 energy dispersive X-ray spectroscopy (EDS) system and						
216	Oxford Instruments AZtec 3.0 nano-analysis software, located in CMCA.						
217							
218	3. Context						
219	3.1. Regional setting						
220	The c. 3.46 Ga Apex Basalt is found in the East Pilbara terrane of the Pilbara Craton,						
221	Western Australia (Fig. 1). This c. 3.53–3.23 Ga terrane contains some of Earth's						
222	oldest and best-preserved rocks, and comprises a series of domed granitoid						
223	complexes, intruded into and overlain by volcano-sedimentary rocks of the Pilbara						
224	Supergroup (Van Kranendonk et al., 2007; Hickman, 2008, 2012). The Pilbara						
225	Supergroup is divided into three unconformity-bound lithostratigraphic groups						

226 (Warrawoona, Kelly, and Sulfur Springs). These crop out across c. 20 greenstone 227 belts in the East Pilbara, each belt dipping away from the granitoids (Van Kranendonk 228 et al., 2001; Hickman, 2012). The lowermost of these groups, containing the Apex 229 Basalt, is the Warrawoona Group, a 10-15 km thick volcano-sedimentary succession 230 deposited between c. 3.53 and 3.43 Ga, dominated by extrusive volcanic rocks with 231 minor interstratified chert, barite, carbonate and volcaniclastic units (Hickman, 1983; 232 Van Kranendonk et al., 2007). The Apex Basalt is best exposed in the Marble Bar 233 greenstone belt where it is c. 3 km thick; here it overlies the Marble Bar Chert 234 member of the c. 3.47 Ga Duffer Formation and is in turn overlain by felsic volcanics 235 of the c. 3.45 Ga Panorama Formation (Van Kranendonk, 2006). 236 237 3.2. Chinaman Creek Geology

238 In the vicinity of Chinaman Creek, approximately 5 km west of Marble Bar, thick 239 extrusive accumulations of pillow basalt and komatiite are punctuated by a 240 weathering-resistant ridge of stratiform chert and associated volcaniclastic rocks, informally referred to as the 'Apex chert' (Fig. 2). The stratiform chert (unit 4 of 241 242 Brasier et al., 2005, 2011), the lowermost and thickest of several stratiform cherts in 243 the Apex Basalt (Kato and Nakamura, 2003), is a 10-15 m thick unit of banded iron-244 rich and iron-poor chert (cf. banded iron formation) of variable texture, composition 245 and colour. Brasier et al. (2005, 2011) recognized that the stratiform chert ridge was 246 separated into three structural blocks (naming them the North, Central and South 247 blocks) by listric normal growth faults. They also showed that, stratigraphically below 248 the ridge, a series of hydrothermal black chert veins cut up through the lower portions 249 of the Apex basalt for up to 1600 m (Figs. 2-3). The veins are particularly thick (up to 250 c. 5 m in diameter) along the growth faults and one such vein (N1 of Brasier et al.,

251 2005; Fig. 3) contains the filamentous microfossil-like artifacts described by Schopf 252 (1993), at a depth of c. 100 m below the palaeosurface. The black chert veins inter-253 finger with, but do not pass through, the upper stratigraphic limit of the stratiform 254 chert (Brasier et al., 2005; Van Kranendonk, 2006) indicating that they are 255 syndepositional with, or penecontemporaneous to, this unit (Fig. 3). Large clasts of 256 both hydrothermal black chert and stratiform chert are found in the overlying 257 pyroclastic breccia bed (unit 5 of Brasier et al., 2005, 2011) indicating that both were 258 lithified prior to the commencement of the next volcanic cycle. In the vicinity of these 259 veins, the stratiform chert can be highly brecciated with dilatational black chert 260 artificially thickening the stratiform succession and creating angular blocks of bedded 261 chert that appear to 'float' in black chert (Brasier et al., 2005), confirming that at least 262 some of the stratiform chert must predate the black chert. Stratiform material may also 263 be found entrained at depth (up to c. 150 m) within the black chert veins, likely 264 caused by either vigorous downward convection during hydrothermal fluid flow or 265 phreatomagmatic explosions (Van Kranendonk, 2006). In contrast to most previous 266 studies that have sought to address the origin of carbonaceous structures in and 267 around the hydrothermal veins (Wacey et al., 2015; Bower et al., 2016 and references 268 therein), here we focus on stratiform chert that shows evidence for sedimentary 269 structures, and mostly crops out some distance away from the major hydrothermal 270 veins (Fig 3).

271

272 **4. Results**

273 4.1. Petrographic division of stratiform chert types

274 The stratiform chert is present in each of the three structural blocks at Chinaman

275 Creek, but is most continuous in the north and south blocks. The central block has a

276 comparative paucity of both stratiform and hydrothermal chert. We here divide the 277 stratiform chert at Chinaman Creek into five distinct types on the basis of 278 petrographic observations: silicified volcaniclastics (mostly layered ash and 279 agglomerate; Fig. 4a-b), clotted carbonaceous chert (Fig. 4c-d; cf. Lowe and Knauth (1977), banded microgranular chert (Fig. 4e-f; Supp. Figs. 1-2), metalliferous, mostly 280 281 iron-rich chert (Fig. 4g-h) and banded black, grey and white chert (Fig. 4i-j). 282 283 This study focuses on the banded microgranular cherts, which not only preserve 284 significant quantities of carbonaceous material, but also show clear sedimentary 285 textures, such as grain orientation and sorting (Fig. 4e; Supp. Figs. 1-2). This is 286 particularly apparent for the largest grains in the microgranular chert (Supp. Fig. 2). 287 Other chert types are currently under detailed investigation but are beyond the scope 288 of this study. The microgranular cherts provide the widest range of carbonaceous 289 textures, though some of these are shared with other chert types: for example, 290 laminated textures on the mesoscale define the fabrics of parts of the microgranular

291 chert, plus parts of the black, grey and white and iron-rich banded cherts. However,

292 microscopic laminations within individual grains are solely found within

293 microgranular cherts. Well-developed spherulitic silica textures characterise the

clotted carbonaceous cherts, but are also minor components of the microgranular andother cherts.

296

297 4.2. Microgranular chert fabrics

Fabrics within the microgranular cherts are variable, even on the scale of a singlestandard thin section and include (i) microgranular zones, (ii) laminated textures and

300 (iii) spherulitic textures, which we address in order below. Additionally, μ m-mm scale

301 post-depositional micro-quartz and macro-quartz veins represents multiple later

302 episodes of veining. Brecciation of cherts is common around the large hydrothermal

303 intrusive black chert veins, however, data herein come from non-brecciated stratiform

- 304 chert away from macro-scale veins.
- 305
- 306 4.2.1. Microgranular zones and grain types

307 Microgranular zones comprise grains of various shapes and sizes that show some

308 degree of sorting and a preferred orientation (Fig. 4e-f; Supp. Figs. 1-2). These zones

309 show colour banding in roughly equal proportions of light and dark material (cf.

310 'laminated silty argillites' in Cressman, 1989; Scheiber, 1990; Scheiber et al., 2012);

311 optically lighter and darker bands alternate on the sub-millimetre- to millimetre-scale,

and have markedly differing characters (Fig. 4e-f; Supp. Fig. 1). Microgranular cherts

are generally well-sorted and usually grain-supported, though lobate grain-rich layers

are locally matrix-supported, principally through their high interparticle porosity.

315 Subtle imbrication of grains is present, especially in elongate flakes. This lithology

316 superficially resembles a fine-grained, shallow-water grainstone or pelsparite, though

317 is more compositionally akin to a silicified shale (Schieber et al., 1990).

318

319 The most common components of the microgranular chert are sub-rounded,

320 carbonaceous lobate grains or 'fluffs' (Fig. 5a-b). These range from $< 100 \ \mu m \ to > 1$

321 mm in size, with similar sizes of fluffs tending to be spatially correlated, defining

322 discrete domains. The domains are sometimes lense-like indicating a probable

323 sedimentary origin; this might suggest some periodicity to sediment input. Though

324 some fluffs have a high aspect ratio and tapering edges, most are sub-spherical. In all

325 sections, regardless of orientation relative to bedding, these grains have generally

326 cloud-like, 'fluffy' morphologies. They frequently have inclusions of wisps of silica 327 and isolated, euhedral-subhedral opaque crystals, which together constitute < 20 % of 328 the grain (Fig. 5a-b). We interpret these fluffy grains as carbon-impregnated silicified 329 volcanic ash (cf. Lowe, 1999; Brasier et al., 2006). Their considerable interparticle 330 (~30%) and intraparticle porosities supports this hypothesis, as does their multiclastic 331 composite constructions (Fig. 5b), suggesting either in-air clotting of multiple ash 332 grains when moistened or submarine or water-surface moistening and coagulation. 333 Elemental mapping shows elevated concentrations of aluminium and potassium 334 within the fluffy grains (Supp. Fig. 3a), also consistent with an origin as volcanic ash 335 (Nakagawa and Ohba, 2003). Furthermore, these grains strongly resemble silicified volcaniclastics described from other members of both the Warrawoona Group and the 336 337 time-equivalent Onverwacht Group of South Africa (Lowe and Knauth, 1977, 1978; 338 Walsh, 2004; Walsh and Lowe, 1999). Raman micro-spectroscopy confirms the 339 carbonaceous composition of these fluffy grains (Fig. 5c) and shows that carbon 340 impregnation occurred prior to the maximum metamorphic or hydrothermal heating of 341 these rocks in the early-mid Archean (Fig. 5d).

342

343 The second most common grain type, accounting for approximately 30% of most 344 microgranular cherts, is the 'flake', which is a considerably darker, tapered, elongate 345 grain (Fig. 6a-c). Most flakes are shallowly curved (Fig. 6c); since no way-up criteria 346 are available in what we here interpret as a reworked sediment, no inference of 347 concavity or convexity is implied. Flakes are largely restricted to the microgranular 348 chert, suggesting either a transient formational mechanism, or small reservoir of 349 material from which flaky grains can be drawn, preventing more widespread 350 preservation. Flaky grains appear more densely carbonaceous than fluffy lobate

351	grains, and resemble either: i) ripped-up slivers and laminae of fine-grained sediment						
352	(cf. Schieber et al., 2012); ii) ripped-up chips of microbial mats (Noffke, 2010 and						
353	references therein); or iii) compressed fluffy grains. Where thin sections are cut						
354	perpendicular to the macroscopic banding, there is an obvious preferred orientation of						
355	elongate clasts, which is lost in thin sections cut parallel to macroscopic banding.						
356	These oriented flakes usually dominate granular layers alternately to the						
357	aforementioned fluffs (Fig. 4e). Raman micro-spectroscopy confirms the dominantly						
358	carbonaceous composition of flaky grains (Fig. 6a-b), and the carbon 'D' and 'G'						
359	peak intensities, position and shapes of these grains are identical to the						
360	aforementioned fluffy grains.						
361							
362	One explanation for the flaky grains is that they are compressed lobate fluffy grains.						
363	Rare, partially compressed fluffy grains are observed in silicified ashes at Chinaman						
364	Creek; these have tapering margins and jagged bifurcations and compaction is						
365	suggested by sutured contacts between adjacent grains (Fig. 6d). However, such						
366	compressed lobate clasts with sutured margins have not been observed in the						
367	microgranular chert. In addition, when the intra-grain features of known compressed						
368	lobate clasts (Walsh and Lowe, 1999) are compared to the flaky grains in the						
369	microgranular cherts, the two bear only superficial morphological resemblance. For						
370	example, inclusions are rare to absent in the flaky grains described herein, but are						
371	common in known compressed lobate clasts. Grain morphologies of the flaky grains						
372	suggest a more linear, fissile breakage than the irregular outlines of high aspect ratio						
373	lobate grains (Walsh and Lowe, 1999). Flaky grains also appear to lack the						
374	enrichment in aluminium and potassium observed in the fluffy grains (Supp. Fig. 3).						
375	Furthermore, the occasional occurrence of flaky grains immediately adjacent to						

uncompressed fluffy grains within a sediment layer (Fig. 6b) discounts a mechanism
whereby changes in silicification style may allow one layer to remain uncompressed
(fluffy grains) while the next layer becomes compressed (flaky grains).

379

An alternative mechanism for the generation of flakes can be found in modern flume experiments on very fine-grained sediments. These suggest that above a certain flow velocity threshold, flake-like fragments of sediment can be removed from watersaturated muds, and redeposited as flakes once flow velocity dissipates (Schieber et al., 2012). A similar mechanism could also explain flake genesis as fragments of microbial biofilms eroded off the edges of a larger parent mat (cf. Noffke et al., 2013 fig. 17).

387

The final type of clast found in microgranular cherts is the laminated grain (Figs. 7-8, Supp. Fig. 2); these are much rarer, making up < 5 % of chert volume. Laminated grains can be separated into two categories: i) those which are inherently laminated, i.e. primary lamination (Fig. 7), and ii) those which show lamination resulting from secondary intrusion or dilation by silica, either from the matrix, or from later clear microcrystalline veins (Fig. 8). Both are described in more detail in section 4.2.2.1 below.

071

395

396 4.2.2. Laminated textures

397 Lamination occurs on a variety of scales. The microgranular cherts are

398 laminated on the mm-scale and these laminae appear to be defined by the

relative proportions of fluffy and flaky grains (Fig. 4e, Supp. Fig. 1). Laminae

400 also occur within single, albeit rare, grains in the microgranular chert (Figs. 7-8,

401 Supp. Fig. 2), mostly being defined by the relative proportions of carbon and

402 silica at the tens of microns scale (see section 4.2.2.1 below). Finally,

403 carbonaceous laminae can persist across entire thin sections cut perpendicular to

404 bedding, and can be stacked together vertically for several millimetres in chert

405 zones adjacent to microgranular zones (Fig. 9; see section 4.2.2.2 below). Some

406 of these laminae appear filament-like (cf. Noffke, 2009, 2010) rather than being

407 layered planar surfaces.

408

409 4.2.2.1. Laminated grains

410 Primary laminated grains: Primary laminated grains within the microgranular chert 411 feature gradation between their alternating siliceous and carbonaceous laminae. They 412 display an ordered repetition of lamination that could indicate either an environmental 413 or biological periodic oscillation acting on the precursor sediment. Dark carbonaceous 414 and pale siliceous laminae occur sequentially on the scale of tens of microns, with 415 neither predominating (Fig. 7a-d). Raman micro-spectroscopy confirms that the dark 416 bands are indeed carbonaceous (Fig. 10b) while NanoSIMS ion mapping shows that 417 carbon, nitrogen and sometimes sulfur co-occur in enhanced concentration in dark 418 laminae (Fig. 11). The Raman spectra (Fig. 10c) show that the thermal maturity of the 419 carbon is consistent with an early Archean age of deposition. The Raman spectra are 420 qualitatively near identical to those described previously from the stratiform Apex 421 chert (Sforna et al., 2014). It is not possible to compare our spectra quantitatively with 422 those of Sforna et al (2014) because we used a different laser wavelength (785 nm as 423 opposed to 514 nm) for excitation of the sample, which has been shown to induce a 424 shift in the carbon D peak position (Pocsik et al., 1998). Hence, our Raman data only 425 confirm that the carbon in the laminae experienced a similar degree of heating to

previously reported carbon, hence is likely an early phase, but cannot distinguish
whether the carbon was sourced from a biological or other (e.g., deep hydrothermal)
reservoir.

429

430 One character common to all of the grains herein interpreted as primarily laminated is 431 that their laminae are non-isopachous, with thickness varying significantly over tens 432 of microns along bands (Fig. 7). Many laminated grains show a thickening of the 433 carbonaceous material toward the 'crests' of individual gently undulose laminae (Fig. 434 7). Some grains demonstrate particularly undulose and wrinkled laminations (Fig. 7) 435 and/or the rolling-up of multiple laminations (Figs. 7b, 12). Siliceous bands exhibit a 436 crystallisation texture that appears to be influenced by the adjacent carbonaceous 437 material - for example, malformed growth of otherwise euhedral microquartz crystals, 438 further suggesting that carbonaceous laminae were likely lithified in their non-439 isopachous form.

440

441 The three-dimensional morphology of carbonaceous material in laminated grains is 442 highlighted by autofluorescence under confocal laser scanning microscopy (CLSM), 443 which demonstrates a wrinkled planar form (Fig. 13; supplementary movie 1) i.e., it is 444 neither filamentous nor tubular. Many of the thicker carbonaceous bands appear 445 multi-laminar in both light microscopy (Fig. 7d) and CLSM (Fig. 13). The largest laminated grain examined by CLSM (from locality CC8 of Brasier et al., 2011) 446 447 reveals the rolling up of the tapering ends of several laminae; in some cases, these 448 almost roll over by 180° (Fig. 13c-d; supplementary movie 1). Rollups such as these 449 have been proposed as evidence for an initial plasticity of structure and are commonly 450 associated with ancient microbial mats (Tice & Lowe, 2004; Tice et al., 2011). Roll451 up formation is thought to begin with the erosion, by waves, tides, or other marine 452 current movements, of the original mat. This releases fragments of the mat and leaves 453 tear-up structures in the remaining microbial edifice (Westall et al., 2015). Current 454 movements have a range of erosional outcomes, depending foremost on the 455 morphology and geometry of the microbial mat (Tice et al., 2011). However, if an 456 eroded mat fragment is glutinously bound by cohesive extra-cellular polymeric 457 substance (EPS), current action will deform, but not structurally disintegrate, the 458 fragment, reworking it into a roll-up (cf. Tice and Lowe, 2004).

459

460 Secondary laminated grains: Some laminated grains appear secondary in nature and 461 more closely resemble fragmented flakes. Here, micro-quartz veins traverse and 462 intrude the clast disconformably, resulting in sharp contrasts between laminae (Fig. 463 8a-c). The repetitively alternating banding characteristic of primary fabrics is not 464 present. If these laminae were syn-sedimentary or biologically mediated, a gradation 465 between carbonaceous and siliceous layers would be expected, as observed in the 466 previously described primary grains, and indicative of incremental growth of the 467 precursor sediment and/or biological system. The lamina boundaries here, however, 468 are distinct, signifying brittle breakage or intrusion. Where 'gradation' at the margins 469 of laminae is noted, higher magnification observation reveals this to be a result of 470 secondarily loosened darker grains from the adjacent carbonaceous material, likely 471 through pervasive silicification enhancing fracture defects (Fig. 8c). The formational 472 process for these laminated grains is best explained as the intrusion of siliceous fluids 473 into planes of weakness or fracture in the precursor clast, forcing material apart. This 474 process is supported by two further lines of evidence, in addition to the sharp laminar 475 edges. Firstly, the lighter, siliceous bands do not always traverse the entirety of the

476 clast (i.e., there are not always continuous planes as would be expected for a 477 microbial mat or regularly repeating sediment deposition) and are aligned randomly 478 (i.e., they are not likely related to the primary laminated fabric of the microclastic 479 chert). Secondly, the undulations of the carbonaceous laminae appear to be an 480 intimately related response to forcing caused by intercalated growth of silica: there is 481 a near perfect fit between now-separated flakes which leads to our interpretation of 482 these fragments as having once been parts of a larger precursor grain (see particularly 483 the central and lower major grains in Fig. 8a).

484

485 Other laminated grains: Some of the most finely laminated grains fit into neither of 486 the aforementioned categories. In these cases, laminae are distinctly isopachous, have 487 tapered edges, and can be discontinuous across a clast. In contrast to all other laminae, 488 these are composed of very fine yellow and orange-brown grains, only visible at high 489 magnification (Fig. 8d). Carbonaceous material is absent, and these grains show 490 strong resemblance to tubular pumice or welded tuff (cf. Klug et al., 2002; Polacci, 491 2005). Similar microstructures have also been observed in stratigraphically higher 492 Apex Basalt (Matthewman, pers. comm.).

493

494 4.2.2.2. Mesoscopic 'filament-like' laminations

495 At two localities (CC164 and CCT23 of Brasier et al., 2011), mesoscopic laminations

496 occur in microcrystalline black-grey-white chert zones (we interpret this lithology as

an end-member classification of microgranular chert, and it should not be confused

498 with the black-grey-white banded cherts, which are independent) adjacent to

499 microgranular zones. These comprise narrow filament-like textures with an

500 undulating, wrinkled topography (Fig. 9b, dashed arrows). The laminae are stacked

501 vertically into packages varying from $< 100 \mu m$ to several millimetres thick. 502 Individual filament-like laminae within each package are rather diffuse, but the best-503 preserved examples are about 10-20 µm thick (Fig. 9d, dashed arrows). The lateral 504 extent of these laminae can be as little as a few tens of micrometers or they may 505 persist across an entire thin section (Fig. 9a) or hand specimen. Laminae are 506 interspersed with microcrystalline silica and this overall texture is sometimes cross-507 cut by later micro-quartz veins. A number of aggregations of these laminae appear to 508 entrain orientated detrital sediment grains (Figs. 9c-e, 14). Raman micro-spectroscopy 509 confirms that the laminations are carbonaceous, that the carbon is not a modern 510 contaminant, and that the trapped grains are quartz (Fig. 14). This is consistent with 511 the trapping and binding of sediment grains by filamentous microbes and their 512 associated exopolymeric substances, as observed in modern microbial mats, and 513 several fossil examples of Archean age (e.g., Noffke et al., 2001, 2003, 2013; Westall 514 et al., 2011).

515

516 4.2.3. Spherulitic textures

517 The stratiform cherts are often punctuated by spherulitic features. For example, 518 irregular shapes exhibited by some carbonaceous fluffy grains in clotted and 519 microgranular cherts - shapes in marked contrast to the dominant sub-rounded, cloud-520 like morphologies of these grains - could result from their fragmentation by silica 521 spherules. Fragmentary, homogeneous, and indistinct carbonaceous clasts are often 522 present around lobate grain margins in zones of spherulitic alteration; these may 523 signify the breakup products of larger lobate parent bodies by spherulitic silica 524 growth. These spherulitic textures are often associated with elongate, sometimes 525 partially-filamentous fragments of carbon, that resemble abiogenic pseudofossils

526 previously identified in the black chert veins below the stratiform chert (Brasier et al.527 2005, 2011).

528

529 **5. Discussion**

530 5.1. Assessment of Biogenicity

531 A number of the carbonaceous microstructures detailed above are comparable to 532 features previously interpreted as biosignatures in Archean and Proterozoic rocks 533 (e.g., Noffke et al., 2003, 2006, 2013; Tice and Lowe, 2004). Microstructures of 534 particular interest identified through our appraisal of the stratiform Apex chert are: i) 535 primary laminated grains; ii) filament-like laminae entraining sediment grains; iii) 536 roll-up structures; and iv) flaky grains. Combined, these microstructures resemble a 537 suite of microscopic microbially induced sedimentary structures (MISS) as defined by 538 Noffke (2009, 2010), and described from both modern (e.g., Noffke et al., 2001) and 539 ancient (e.g., Noffke et al., 2003) environments. Here we test the biogenicity of these 540 Apex microstructures against a suite of biogenicity criteria (e.g., Schopf and Walter, 541 1983; Buick, 1990; Brasier et al., 2004; Hofmann, 2004; Wacey, 2009; Noffke 2010). 542 Some of these criteria are specific to MISS, whilst others are more generic, applicable 543 to any putative Precambrian biogenic structure. The 'fluffy' grains, spherulitic 544 microstructures and secondarily laminated grains will not form a substantial part of 545 our discussion because there is little or no suggestion from their morphology that they 546 might be biogenic. They are, however, useful as comparative material in our 547 discussion of the putatively biogenic microstructures.

549 i) Biogenic structures must occur in rocks of both known provenance and of
550 demonstrable Archean age. Furthermore, the structures must be a part of, and
551 syngenetic with, the primary fabric of the host rock.

552 The stratiform 'Apex chert' has been extensively mapped from the kilometre down to 553 the micrometre scale, and all samples can be relocated using their GPS coordinates. It 554 is a sedimentary unit, cropping out for several hundred metres along strike, and is 555 located within a well-constrained stratigraphic column, with radiometric dates from 556 both above and below the unit (e.g., Van Kranendonk, 2006). The microstructures of 557 interest occur either within grains and clasts that have been eroded from older units 558 and then incorporated into the microgranular chert (e.g. primary laminated grains), or 559 are part of the primary fabric of the rock (e.g. mesoscopic 'filamentous' laminations). 560 Raman micro-spectroscopy shows that all carbon has a thermal maturity consistent 561 with an early Archean age (i.e. emplacement prior to peak metamorphic/hydrothermal 562 temperatures experienced by the Apex succession sometime prior to 3 Ga; Van 563 Kranendonk, 2006; Sforna et al., 2014) thus cannot be a more modern contaminant. 564

565 ii) Biogenic structures should not be found in metastable mineral phases, void566 filling cements or veins.

None of the microstructures of interest are found in such late-stage or metastable mineral phases; they occur either in clasts of micro-quartz that were lithified, eroded and reworked prior to the final lithification of the stratiform chert (e.g., Fig. 5a), or are found in primary laminated chert (e.g., Fig. 9). In contrast, spherulitic textures forming filamentous and other carbonaceous fragments are found in void filling cements and cross-cutting veins. These are demonstrably crystal-edge effects, usually resulting from the growth of silica spherules. The carbon in such later phases has been

- redistributed to such an extent that its morphology cannot be used to determine itsorigin (cf. Pinti et al., 2009; Wacey et al., 2015).
- 576

577 *iii)* Fossil MISS must occur in sedimentary rocks having undergone only low grades
578 of metamorphism.

- 579 This criterion is met by the sedimentary sequences in the Marble Bar greenstone belt,
- 580 which have not experienced more than lower greenschist facies regional
- 581 metamorphism (Hickman and Lipple, 1978; Van Kranendonk, 2006). More
- specifically, a recent Raman study at the Chinaman Creek locality estimated that the
- 583 maximum temperatures experienced by these rocks were between 265°C and 360°C,
- 584 which may represent the peak temperature of regional metamorphism and of
- 585 hydrothermal fluids respectively (Sforna et al., 2014). Multiple potential biosignatures
- 586 have been reported previously from similarly silicified sediments of the Pilbara craton
- 587 (e.g., Sugitani et al., 2010, Wacey et al., 2011; Noffke et al., 2013) indicating that
- 588 MISS could also be preserved within the stratiform Apex chert.
- 589
- 590 iv) The geological context of the lithology should be plausible for life; ideally, the
 591 lithology should indicate a transgressive depositional phase, since this is the
- 592 *environment in which modern MISS develop.*
- 593 The stratiform Apex chert is likely to represent a quiescent marine environment in
- which low-density particles can settle out of suspension, i.e. lobate ash clasts in layers
- and very fine clay or fragments of microbial mat. Water temperatures would be within
- the range in which (hyper)thermophilic life could flourish; geochemical evidence,
- 597 including relatively high concentrations of barium in the stratiform chert and small
- 598 positive europium anomalies, indicate low-temperature (100-150°C) hydrothermal

venting (Kato and Nakamura, 2003). In addition, the input of volcanic detritus may
have provided essential elements for life, thus the environment appears habitable.
However, further high-resolution sedimentary logging is required to determine
whether a transgression can be identified within the stratiform chert unit. This work
should also search for evidence of macroscopic MISS that are as yet unreported from
this unit.

605

606 v) MISS are predominantly preserved in fine quartz-rich sediments in a moderately
607 reworked hydraulic setting.

608 The stratiform Apex chert partially meets this criterion, especially for the

609 microgranular cherts (e.g. localities CC8 and CC117 of Brasier et al., 2011), which

610 are interpreted as reworked sediments. The Apex stratiform rocks now have an almost

611 uniform quartz composition. However, since widespread silicification has altered their

original composition, this implies little regarding deposition in a siliciclastic system.

613 Initial grain size is also difficult to determine, having been extensively modified by

614 various silicification events, though the rare trapped grains in the filament-like lamina

615 (Fig. 9) are comparable in size to those found in other Archean and Proterozoic MISS

616 (e.g., Noffke et al., 2003, 2006, 2013).

617

618 vi) Structures should fit into a plausible evolutionary context and would ideally

619 *exhibit community behavior.*

620 Microbial mats are demonstrably one of the most ancient and enduring biological

621 communities, with evidence of microbial mat/sediment interaction reported from

622 rocks of similar age to the Apex chert in both the Pilbara and Barberton regions (e.g.,

623 Tice and Lowe, 2004; Allwood et al., 2006; Westall et al., 2001, 2006, 2015; Noffke

624 et al., 2013). An interpretation of the laminated and filamentous Apex microstructures 625 as MISS fits within this evolutionary context and, by analogy to modern ecosystems, 626 implies community behavior of a microbial mat (Noffke, 2008; Schieber et al., 2007). 627 We do not interpret any of the microstructures as microfossils, though we raise the 628 possibility that the filament-like laminae entraining sediment grains may be the 629 diffuse remnants of mat-building filamentous microorganisms (cf. Noffke et al., 630 2003). Further detailed geochemical and morphological research must be conducted 631 into these, however, before such an interpretation can be substantiated. 632 633 vii) Laminated MISS should be wavy or wrinkled, with several orders of curvature

634 i.e. should not be uniform crusts, which are usually precipitative. Thickening of
635 carbonaceous laminae towards the crests of laminae would provide additional
636 evidence of biology (cf. Pope and Grotzinger, 2000).

637 Both the primary laminated grains and the filament-like laminae are often wavy and 638 wrinkled at the mesoscopic and microscopic scale (Figs. 7, 9, 12-14). In addition, 639 some of the laminae within larger grains in the microgranular chert thicken toward 640 undulose crests. In contrast, such features are absent from the secondarily-laminated 641 carbonaceous grains (Fig. 8a-c) and from isopachous microstructures here interpreted 642 as tubular pumice (Fig. 8d). Within the metalliferous cherts and black, grey and white 643 banded cherts (Fig. 4g-j), there are laminations that are continuous across thin 644 sections, often on the same sub-millimetre scale as the laminae described in the 645 microclastic cherts, These laminae are, however, isopachous and show nothing of the 646 multiple orders of curvature required for a biological interpretation. Hence, they are 647 interpreted as precipitative crusts growing sequentially over other fabric elements in

648 the cherts.

- 650 ix) *MISS must be shown to preserve textures that either represent, have been caused*651 *by, or are related to, biofilms or microbial mats.*
- In addition to the wavy and wrinkled laminae described above, some of the putative
- 653 MISS contain grains around which the filament-like laminae wrap. In modern
- biofilms, microbial mats and stromatolites, such microstructures form via the trapping
- and binding of sediment grains by 'sticky' filamentous microorganisms and their
- associated extra-cellular polymeric substances (EPS; e.g., Reid et al., 2000).
- 657 Similarly, rolled-up microstructures in modern settings are cited as evidence of an
- 658 initial plasticity, hence cohesiveness in the sediment, and ancient examples have been
- 659 interpreted as resulting from the interaction of erosive forces, such as currents, with a
- 660 microbial mat (e.g., Tice and Lowe, 2004). We have identified putative roll-ups in the
- 661 microclastic cherts (CC8 and CCT27), though they are of smaller size than well-
- accepted Archean examples (Tice and Lowe, 2004). Additionally, a plausible
- 663 interpretation of the flake-like grains reported here is that they are micro-scale
- analogues of microbial mat chips commonly found in modern MISS assemblages,
- also formed when water agitation (driven by tides or storms, for example) tears small
- 666 pockets of semi-cohesive material from their parent microbial mat (Gerdes and
- 667 Krumbein, 1987, Tice et al., 2011).
- 668
- 669 x) MISS should possess geochemical signals indicative of biology
- 670 Both laser Raman micro-spectroscopy and NanoSIMS data show that the laminated
- 671 microstructures are carbonaceous. The Raman spectra are consistent with previous
- data from ancient biological material within greenschist facies rocks (e.g., Tice et al.,
- 673 2004) and with previous data from the Apex stratiform chert (Sforna et al., 2014).

674 Raman data cannot prove the biogenicity of organic material, because similar spectral 675 features can be obtained from non-biological organic matter (Pasteris and Wopenka, 676 2003). NanoSIMS data show the co-occurrence of carbon, nitrogen and sometimes 677 sulfur within the dark laminae of primary laminated grains. These data are not 678 quantitative, but they do demonstrate that three of the elements integral to life occur 679 in elevated concentrations in zones that also have a microbial mat-like morphology. 680 Similar correlations of microbial morphology with biologically significant elements 681 have been demonstrated within modern and ancient stromatolites (Wacey, 2010) and 682 bona fide Precambrian microfossils (Oehler et al., 2006; Wacey et al., 2011).

683

684 5.2. Summary of potential biogenicity

685 Of the range of textures exhibited by the stratiform cherts, we find that it is the 686 microgranular cherts that hold the most promise for the retention of biosignatures. 687 Primary laminated grains, filament-like wrinkle structures, roll-ups, and flaky grains 688 may all plausibly be interpreted as remnants of a microbial mat community. The 689 texture of the microclastic cherts suggests a shallow, quiescent environment of 690 deposition, in which weak but persistent currents facilitated the orientation and 691 imbrication of elongate clasts. There is a prominent volcaniclastic component to the 692 microgranular cherts, and evidence of a proximal silicic source comes in the form of interbedded silicified ashes and other volcaniclastics that constitute much of the 693 694 stratiform stratigraphy at Chinaman Creek (Kato and Nakamura, 2003; Brasier et al., 695 2011). It may be that this volcanic input provided elements, particularly metals, 696 significant to the emergence of life in this habitat (cf. Barras, 2012; Van Kranendonk, 697 2006). However, the lack of evidence for macroscopic MISS or definitive 698 microfossils in this unit urges a note of caution. In addition, the environment of

deposition and hydrothermal style of silicification (e.g., Kato and Nakamura, 2003),

700 overprinting some of the primary sedimentary features, is rather different from that of

traditional siliciclastic settings in which MISS are well understood (cf. Noffke, 2010),

and for which the criteria outlined above were primarily designed.

703

704 Other lithologies in the stratiform sequence at Chinaman Creek, namely banded grey 705 and white and metalliferous cherts, clotted carbonaceous cherts and silicified 706 volcaniclastics, are more difficult to decode. They have not yet provided putative 707 biogenic structures, though they are important for diagnosing environmental and 708 redox conditions during Apex time. The clotted cherts, in particular, possess textures 709 generated from spherulitic silica growth, during which microfossil-like artifacts 710 developed around the margins of crystals. The carbon in these textures may ultimately 711 have a biogenic origin, but abiogenic sources, for example through hydrothermally-712 mediated processes (e.g., Fischer-Tropsch synthesis), remain an equally plausible 713 explanation for this carbon (cf. Brasier et al., 2005). 714 715 This study adds to the growing evidence for a diversity of primitive life in the early 716 Archaean era, and provides a detailed assessment of carbonaceous microstructures 717 within the stratiform Apex chert at Chinaman Creek, a lithology that has been only

very briefly described in previous work (e.g., Brasier et al., 2011; Sforna et al., 2014).

719 Our data support the hypothesis that shallow-water environments, together with input

from volcanic and hydrothermal sources, were likely pivotal niches occupied by

simple, prokaryotic mat-forming organisms. The MISS-type structures described

herein are found in relatively close proximity to penecontemporaneous hydrothermal

fabrics, yet have no apparent genetic association with these higher-temperature

events; thus their interpretation as biological signals is more probable than an abioticorigin.

726

727 **5.** Conclusions

The stratiform 'Apex chert' at Chinaman Creek is a varied and previously

vulture relation of the second second

based on petrographic observations: i) carbonaceous laminated microgranular chert;

ii) laminated black, grey and white chert; iii) metalliferous (Fe-rich) chert; iv) clotted

carbonaceous chert; and v) silicified volcaniclastics. The protoliths of all stratiform

chert rocks have been pervasively and ubiquitously silicified, and a dominant

component of this silicification was low temperature (100-150°C) hydrothermal fluids

735 (Kato and Nakamura, 2003).

736

737 The macroscopic sedimentary textures of the stratiform Apex cherts, which have 738 dominant silt-grade grains in most localities studied, and occasional imbrication of 739 semi-lithified chert fragments, hints at a shallow marine depositional environment. 740 The poor lateral continuity of individual chert layers argues against deep marine 741 pelagic settling of sediment. The depositional environment is herein interpreted to be 742 a protected shallow marine environment, where weak currents are intermittently 743 present to sort and orient clasts. Inter-bedded metalliferous cherts, either ferruginous 744 or jaspilitic, may signify a change in redox state or temperature, most likely linked to 745 the penecontemporaneous hydrothermal venting and the intrusive black chert veins 746 (Kato and Nakamura, 2003; Brasier et al., 2005, 2011). Volcanic components, largely 747 ashfall, are prevalent throughout the stratiform sequence, consistent with a shallow-748 marine environment situated adjacent to active volcanoes. This is similar to the

749 environmental setting described for other units from both the Pilbara and Barberton 750 regions containing putative biological remains of approximately equivalent age (e.g., 751 Kitty's Gap Chert and Josefsdal Chert; Westall et al., 2006, 2011, 2015). The 752 stratiform Apex chert depositional environment is not compatible with the deeper 753 marine regime suggested for some Archean cherts (Lowe, 1984; Paris et al. 1985). 754 755 Carbonaceous material is especially abundant in the microgranular and clotted cherts, 756 and is particularly concentrated in grains. Carbonaceous textures interpreted to have a 757 biological component are present in the microgranular cherts as four morphotypes. 758 Firstly, there are carbonaceous laminated grains that pass multiple geological, 759 morphological and geochemical criteria for biogenicity and antiquity. Secondly, more pervasive carbonaceous filament-like laminations are present, which entrain sediment 760 761 grains and closely resemble microscopic MISS. Thirdly, we report elongate, flake like 762 carbonaceous grains, which potentially represent eroded, 'ripped-up' fragments of a 763 microbial mat (cf. Noffke, 2009). We caution that further work is required on the 764 flake-like grains to fully discount an origin from a purely sedimentary protolith (cf. 765 Schieber et al., 2012). Finally, rare roll-up structures are present, both as part of larger 766 laminated grains, and as isolated features in the matrix of microclastic cherts. These 767 are interpreted as current-eroded and plastically reshaped microbial mat fragments, 768 similar to those described from the ~3.4 Ga Buck Reef Chert (Tice and Lowe, 2004; 769 Tice et al. 2011). 770 771 CLSM is here shown to be an effective technique for the imaging of carbonaceous

772 microstructures in these Archean cherts; the autofluorescence of carbonaceous

773 material produces sequential tomograms through the depth of all thin sections

774 investigated herein. This technique enables the generation of sub-micrometer-scale 775 spatial resolution, three-dimensional renderings of features of biogenic interest, and 776 here strengthens the morphological evidence for the biogenicity of some of the 777 described laminated carbonaceous textures. NanoSIMS and laser Raman provide 778 evidence for the concentration of life-significant elements in microstructures that 779 closely resemble the morphology of microbialites. An encouraging combination of 780 both morphology and chemistry pertinent to life in the laminated microstructures of 781 the stratiform cherts, a lithology representing a geologically plausible environment for 782 microbial life, suggests that such features have a biological origin. Although no 783 compelling evidence for life has been found in the underlying heavily studied black 784 chert veins (Brasier et al., 2002, 2005, 2006, 2011, 2015; Wacey et al., 2015; Bower 785 et al., 2016), evidence of an early Archean biological community may yet be present 786 at Chinaman Creek.

787

788 Acknowledgements

789 We are grateful for the assistance of Owen Green and Jeremy Hyde at Oxford 790 University Department of Earth Sciences for the preparation of thin sections for 791 microscopy and discs for NanoSIMS. KHL was supported by Oxford University 792 Department of Earth Sciences master's thesis funding, St Edmund Hall, and by a 793 Gareth Roberts grant. We acknowledge the facilities, scientific and technical 794 assistance of the Australian Microscopy & Microanalysis Research Facility at the 795 Centre for Microscopy Characterisation and Analysis, The University of Western 796 Australia, a facility funded by the University, State and Commonwealth 797 Governments. DW was funded by the European Commission and the Australian 798 Research Council (FT140100321). This is Australian Research Council Centre of

799	Excellence for Core to Crust Fluid Systems publication number XXX (to be filled in
800	on acceptance). Chris Grovenor at Oxford University Department of Materials kindly
801	provided advice and consultation with regard to NanoSIMS and arranged our access
802	to the facilities of the Department of Materials at Begbroke Park, Oxford. RG is a
803	Scientific Associate at the Natural History Museum, London, and a member of the
804	Interdisciplinary Centre for Ancient Life (UMRI), and was an 1851 Royal
805	Commission Research Fellow for the majority of this project.
806	
807	
808	References
809	
810	Allwood, A.C., Walter, M.R., Kamber, B.S., Marshall, C.P., & Burch, I.W., 2006.
811	Stromatolite reef from the Early Archaean era of Australia. Nature 441, 714-718.
812	
813	Barras, C., 2012. Rocky start for life on Earth. New Scientist 18 February 2012, pp 6-
814	7.
815	
816	Bower, D.M., Steele, A., Fries, M.D., Green, O.R., Lindsay, J.F., 2016. Raman
817	imaging spectroscopy of a putative microfossil from the ~3.46 Ga Apex Chert:
818	Insights from quartz grain orientation. Astrobiology 16 (2)
819	DOI:10.1089/ast.2014.1207.
820	
821	Brasier, M.D., Green, O.R., Jephcoat, A.P., Kleppe, A.K., Van Kranendonk, M.J.,
822	Lindsay, J.F., Steele, A., Grassineau, N.V., 2002. Questioning the evidence for
823	Earth's oldest fossils. Nature 416, 78-81.

825	Brasier, M.D., Green, O.R, Lindsay, J.F., Steele, A., 2004a. Earth's oldest (~3.5 Ga)					
826	fossils and the "Early Eden" hypothesis: questioning the evidence. Origins of Life and					
827	Evolution of the Biosphere 34, 257-269.					
828						
829	Brasier, M.D., Green, O.R., McLoughlin, N., 2004b. Characterization and critical					
830	testing of potential microfossils from the early Earth: the Apex 'microfossil debate'					
831	and its lessons for Mars sample return. International Journal of Astrobiology 3, 139-					
832	150.					
833						
834	Brasier, M.D., Green, O.R., Lindsay, J.F., McLoughlin, N., Steele, A., Stoakes, C.,					
835	2005. Critical testing of Earth's oldest putative fossil assemblage from the 3.5Ga					
836	Apex chert, Chinaman Creek, Western Australia. Precambrian Research 140, 55-102.					
837						
838	Brasier, M.D., McLoughlin, N., Green, O.R., Wacey, D., 2006. a fresh look at the					
839	fossil evidence for early Archaean cellular life. Philosophical Transactions of the					
840	Royal Society B 361, 887-902.					
841						
842	Brasier, M.D., Green, O.R., Lindsay, J.F., McLoughlin, N., Stoakes, C., Brasier, A.T.,					
843	Wacey, D., 2011. Geology and putative microfossil assemblage of the c. 3460 Ma					
844	'Apex chert', Chinaman Creek, Western Australia – a field and petrographic guide.					
845	Geological Survey of Western Australia Perth 2011.					
846						

847	Brasier, M.D.,	Antcliffe, J.,	Saunders, M	., Wacey, D	D ., 2015.	Earth's e	earliest fo	ossils

848 (3.5-1.9 Ga): Changing the picture with new approaches and new discoveries.

850

- 851 Buick, R., 1990. Microfossil recognition in Archaean rocks: and appraisal of
- spheroids and filaments from a 3500 MY old chert-barite unit at North Pole, Western
- Australia. Palaios 5 441-449.

- 855 Cockell, C.S., Olsson-Francis, K., Herrera, A., Meunier, A. (2009). Alteration
- textures in terrestrial volcanic glass and the associated bacterial community.
- 857 Geobiology 7, 50-65.
- 858
- 859 Cressman, E.R., 1989. Reconnaissance stratigraphy of the Prichard Formation
- 860 (Middle Proterozoic) and the early development of the Belt Basin, Washington, Idaho,
- and Montana. United States Geological Survey, Professional Paper, 1490.
- 862
- 863 Everall, N. J., Lumsdon, J., & Christopher, D. J., 1991. The effect of laser-induced
- heating upon the vibrational Raman spectra of graphites and carbon fibres. Carbon 29,
- 865 133-137.
- 866
- Furnes, H., Banerjee, N.R., Muehlenbachs, K., Staudigel, H., de Wit, M., 2004. Early
- 868 life recorded in Archaean pillow lavas. Science 204, 578-581.
- 869
- 870 Gerdes, G., Krumbein, W.E., 1987. Biolaminated Deposits. Berlin, Springer-Verlag,
 871 183 p.

⁸⁴⁹ Proceedings of the National Academy of Sciences 112, 4859-4864.

872

Gnaser, H., 2003. Ionization probability of sputtered cluster anions: C n- and Si n-.
Applied surface science 203, 78-81.

875

- Hickman, A.H., 1983. Geology of the Pilbara Block and its environs. Western
- Australia Geological Survey Bulletin 127, 1-268.

878

- Hickman, A.H., 2008. Regional review of the 3426–3350 Ma Strelley Pool
- 880 Formation, Pilbara Craton, Western Australia. West Australia Geological Survey
- 881 Record, 2008, 15.

882

- Hickman, A.H., 2012. Review of the Pilbara Craton and Fortescue Basin, Western
- Australia: Crustal evolution providing environments for early life. Island Arc 21, 1-

885 31.

- 886
- Hickman, A.H., Lipple, S.L., 1978. Explanatory Notes of the Marble Bar 1:250,000

888 Geological Sheet, Western Australia. Perth: Geological Survey of Western Australia,889 24pp.

890

Hofmann, H.J., 2004. Archean microfossils and abiomorphs. Astrobiology 4, 135-136.

- Kato, Y., Nakamura, K., 2003. Origin and global tectonic significance of Early
- Archean cherts from the Marble Bar greenstone belt, Pilbara Craton, Western
- Australia. Precambrian Research 125, 191-243.

898	Kelly, L.C., Cockell, C.S., Herrera-Belaroussi, A., Piceno, Y., Andersen, G.,
899	DeSantis, T., Brodie, E., Thorsteinsson, T., Martiensson, V., Poly, F., LeRoux, X.,
900	2011. Bacterial diversity of terrestrial crystalline volcanic rocks, Iceland. Microbial
901	ecology 62, 69-79.
902	
903	Kelly, L.C., Cockell, C.S., Thorsteinsson, T., Marteinsson, V., Stevenson, J. (2014).
904	Pioneer microbial communities of the Fimmvörðuháls lava flow, Eyjafjallajökull,
905	Iceland. Microbial ecology 68, 504-518.
906	
907	Kilburn, M. R., & Wacey, D., 2011. Elemental and isotopic analysis by NanoSIMS:
908	insights for the study of stromatolites and early life on Earth. In Stromatolites:
909	Interaction of Microbes with Sediments (pp. 463-493). Springer Netherlands.
910	
911	Klug, C., Cashman, K., Bacon, C., 2002. Structure and physical characteristics of
912	pumice from the climactic eruption of Mount Mazama (Crater Lake), Oregon.
913	Bulletin of Volcanology 64, 486-501.
914	
915	Limaye, A., 2012. Drishti: a volume exploration and presentation tool. In SPIE
916	Optical Engineering+ Applications (pp. 85060X-85060X). International Society for
917	Optics and Photonics.
918	
919	Lowe, D.R., 1999. Petrology and sedimentology of cherts and related silicified
920	sedimentary rocks in the Swaziland Supergroup. In Geologic Evolution of the

- 921 Barberton Greenstone Belt, South Africa (ed. D. R. Lowe & G. R. Byerly) 329, 115–
- 922 132. Boulder, CO: Geological Society of America Special Paper.
- 923
- 924 Lowe, D.R., Knauth, L.P., 1977. Sedimentology of the Onverwacht Group (3.4 billion
- 925 years), Transvaal, South Africa, and its bearing on the characteristics and evolution of
- 926 the early Earth. Journal of Geology 85, 699-723.
- 927
- 928 Lowe, D.R., Knauth, L.P., 1978. the oldest marine carbonate öoids reinterpreted as
- 929 volcanic accretionary lapilli, Onverwacht Group, South Africa. Journal of
- 930 Sedimentary Petrology 48, 709-722.
- 931
- 932 Lowe, D.R., Knauth, L.P., 2003. High Archean climatic temperature inferred from
- 933 oxygen isotope geochemistry of cherts in the 3.5 Ga Swaziland Supergroup, South
- 934 Africa. Geological Society of America Bulletin 115, 566-580.
- 935
- 936 Marshall, C.P., Emry, J.R., Marshall, A.O., 2011. Haematite pseudomicrofossils
- present in the 3.5-billion-year-old Apex Chert. Nature Geoscience 4, 240-243.
- 938
- 939 Marshall, A.O., Emry, J.R., Marshall, C.P., 2012. Multiple generations of carbon in
- 940 the Apex chert and implications for preservation of microfossils. Astrobiology 12,
- 941 160-166.

- 943 Marshall, A.O., Marshall, C.P., 2013. Comment on "Biogenicity of Earth's earliest
- 944 fossils: A resolution of the controversy" by JW Schopf and AB Kudryavtsev,

- Gondwana Research Volume 22, Issue 3–4, pp. 761–771. Gondwana Research 23,
- 946 1654-1655.
- 947
- 948 Marshall, C.P., Olcott Marshall, A., 2013. Raman hyperspectral imaging of
- 949 microfossils: potential pitfalls. Astrobiology 13, 920-931.
- 950
- Nakagawa, M., Ohba, T., 2003. Minerals in volcanic ash 1: primary minerals and

volcanic glass. Global Environmental Research 6, 41-51.

- 953
- Nijman, W. de Bruijne, K.C.H., Valkering, M.E., 1998. Growth fault control of Early
- Archaean cherts, barite mounds and chert-barite veins, North Pole Dome, Eastern

956 Pilbara, Wester Australia. Precambrian Research 88, 25-52.

- 957
- 958 Noffke, N., 2009. The criteria for the biogenicity of microbially induced sedimentary
- structures (MISS) in Archean and younger, sandy deposits. Earth-Science Reviews
- 960 96, 173-180.
- 961
- 962 Noffke, N., 2010. Geobiology: Microbial Mats in Sandy Deposits from the Archaean

963 Era to Today. Springer-Verlag, Berlin, Heidelberg 2010.

- 964
- 965 Noffke, N., Gerdes, G., Klenke, T., Krumbein, W.E., 2001. Microbially Induced
- 966 Sedimentary Structures--A New Category within the Classification of Primary
- 967 Sedimentary Structures: Perspectives. Journal of Sedimentary Research 71, 649-656.
- 968

969	Noffke, N., Hazen, R.M., Nhleko, N., 2003. Earth's earliest microbial mats in a
970	siliciclastic marine environment (2.9 Ga Mozaan group, South Africa). Geology 31,
971	673-676.
972	
973	Noffke, N., Eriksson, K.A., Hazen, R.M., Simpson, E.L., 2006. A new window into
974	Archean life: Microbial mats in Earth's oldest siliciclastic tidal deposits (3.2 Ga
975	Moodies Group, South Africa). Geology 34, 253.
976	
977	Noffke, N., Christian, D., Wacey, D., & Hazen, R.M., 2013. Microbially induced
978	sedimentary structures recording an ancient ecosystem in the ca. 3.48 billion-year-old
979	Dresser Formation, Pilbara, Western Australia. Astrobiology 13, 1103-1124.
980	
981	Oehler, D.Z., Robert, F., Mostefaoui, S., Meibom, A., Selo, M., McKay, D.S., 2006.
982	Chemical Mapping of Proterozoic Organic Matter at Sub-Micron Spatial Resolution.
983	Astrobiology 6, 838-850.
984	
985	Pasteris, J.D., & Wopenka, B., 2003. Necessary, but not sufficient: Raman
986	identification of disordered carbon as a signature of ancient life. Astrobiology 3, 727-
987	738.
988	
989	Pinti, D.L., Mineau, R., Clement, V., 2009. Hydrothermal alteration and microfossils
990	artefacts of the 3,465-million-year-old Apex chert. Nature Geoscience 2, 640-643.
991	

992	Pócsik, I., Hundhausen,	М.	Koós,	М.,	Ley,	L.,	1998.	Origin	of the L	peak in the	9
-----	-------------------------	----	-------	-----	------	-----	-------	--------	----------	-------------	---

- Raman spectrum of microcrystalline graphite. Journal of Non-Crystalline Solids 227,1083-1086.
- 995
- 996 Polacci, M., 2005. Constraining the dynamics of volcanic eruptions by
- 997 characterization of pumice textures. Annals of Geophysics (2005).
- 998
- 999 Pope, M.C., Grotzinger, J.P., 2000, Controls on fabric development and morphology
- 1000 of tufa and stromatolites, uppermost Pethei Group (1.8 Ga), Great Slave Lake,
- 1001 northwest Canada, in SEPM Special Publication Carbonate Sedimentation and
- 1002 Diagenesis in the Evolving Precambrian World, J. Grotzinger and N. James (Eds), p.
- 1003 103-122.
- 1004
- 1005 Reid, R.P., Visscher, P.T., Decho, A.W., Stolz, J.F., Beboutk, B.M., Dupraz, C.,
- 1006 Macintyre, I.G., Paerl, H.W., Pinckney, J.L., Prufert-Beboutk, L., Steppe, T.F., Des
- 1007 Marais, D.J., 2000. The role of microbes in accretion, lamination and early
- 1008 lithification of modern marine stromatolites. Nature 406, 989-992.
- 1009
- 1010 Schieber, J., 1990. Significance of styles of epicontinental shale sedimentation in the
- 1011 Belt basin, Mid-Proterozoic of Montana, U.S.A. Sedimentary Geology 69, 297-312.
- 1012
- 1013 Schieber, J., Bose, S., Eriksson, P., Banerjee, J., Sakar, S., Altermann, W., Catuneanu,
- 1014 D., 2007. Atlas of microbial mat features preserved within the siliciclastic rock
- 1015 record. Elsevier Science, Oxford.
- 1016

- 1017 Schieber, J, Southard, J.B., Schimmelmann, A., 2012. Lenticular shale fabrics
- 1018 resulting from intermittent erosion of water-rich muds-interpreting the rock record in
- 1019 the light of recent flume experiments. Journal of Sedimentary Research 80, 119-128.
- 1020
- 1021 Schindelin, J., Arganda-Carreras, I., Frise, E., Kaynig, V., Longair, M., Pietzsch, T.,
- 1022 Preibisch, S., Rueden, C., Saalfeld, S., Schmid, B., Tinevez, J.-Y., White, D.J.,
- 1023 Hartenstein, V., Eliceiri, K., Tomancak, P., Cardona, A., 2012. Fiji: an open-source
- 1024 platform for biological-image analysis. Nature methods 9, 676-682.
- 1025
- 1026 Schopf, J.W., Packer, B.M., 1987. Early Archean (3.3-Billion to 3.5-Billion-Year-
- 1027 Old) Microfossils from Warrawoona Group, Australia. Science 237, 70-73.
- 1028
- 1029 Schopf, J.W., 1992. In The Proterozoic Biosphere: A Multidisciplinary Study, eds.
- 1030 Schopf, J.W., Klein, C. (Cambridge University Press, New York), pp. 179-183.
- 1031
- 1032 Schopf, J.W., 1993. Microfossils of the Early Archean Apex Chert: New Evidence of
- 1033 the Antiquity of Life. Science 260, 640-646.
- 1034
- Schopf, J.W., 1999. Cradle of Life: the discovery of Earth's oldest fossils. Princeton.
- 1037 Schopf, J.W., Kudryavtsev, A.B., Agresti, D.G., Wdowiak, T.J., Czaja, A.D., 2002.
- 1038 Laser–Raman imagery of Earth's earliest fossils. Nature 416, 73-76.
- 1039
- 1040 Schopf, J.W., Kudryavtsev, A.B., Czaja, A.D., Tripathi, A.B., 2007. Evidence of
- 1041 Archean life: stromatolites and microfossils. Precambrian Research 158, 141-155.

1043	Schopf, J.W., Kudryavtsev, A.B., 2009. Confocal laser scanning microscopy and
1044	Raman imagery of ancient microscopic fossils. Precambrian Research 173, 39-49.
1045	
1046	Schopf, J.W., Kudryavtsev, A.B., Sugitani, K., Walter, M.R., 2010. Precambrian
1047	microbe-like pseudofossils: a promising solution to the problem. Precambrian
1048	Research 179, 191-205.
1049	
1050	Schopf, J.W., Kudryavtsev, A.B., 2012. Biogenicity of Earth's earliest fossils: a
1051	resolution of the controversy. Gondwana Research 22, 761-771.
1052	
1053	Schopf, J.W., Kudryavtsev, A.B., 2013. Reply to the comments of DL Pinti, R.
1054	Mineau and V. Clement, and of AO Marshall and CP Marshall on "Biogenicity of
1055	Earth's earliest fossils: A resolution of the controversy" by J. William Schopf and
1056	Anatoliy B. Kudryavtsev, Gondwana Research 22, 761-771. Gondwana Research 23,
1057	1656-1658.
1058	
1059	Sforna, M.C., van Zuilen, M.A., Philippot, P., 2014. Structural characterization by
1060	Raman hyperspectral mapping of organic carbon in the 3.46 billion-year-old Apex
1061	chert, Western Australia. Geochimica et Cosmochimica Acta 124, 18-33.
1062	
1063	Sugitani, K., Lepot, K., Nagaoka, T., Mimura, K., Van Kranendonk, M., Oehler, D.Z.,
1064	& Walter, M.R., 2010. Biogenicity of morphologically diverse carbonaceous

- 1065 microstructures from the ca. 3400 Ma Strelley Pool Formation, in the Pilbara Craton,
- 1066 Western Australia. Astrobiology 10, 899-920.

Tice, M.M., Lowe, D.R., 2004. Photosynthetic microbial mats in the 3,416-Myr-oldocean. Nature 431, 549–552.

1070

- 1071 Tice, M.M., Thornton, D.C.O., Pope, M.C., Olszewsku, T.D., Gong, J., 2011.
- 1072 Archean microbial mat communities. Annual Review of Earth and Planetary Sciences1073 39, 297-319.

1074

- 1075 Van Kranendonk, M.J., Hickman, A.H., Williams, I.R., Nijman, W., 2001. Archaean
- 1076 geology of the East Pilbara Terrane Western Australia a field guide. Geological

1077 Survey of Western Australia Record 2001/9.

1078

- 1079 Van Kranendonk, M.J., 2006. Volcanic degassing, hydrothermal circulation and the
- 1080 flourishing of early life on Earth: A review of the evidence from c. 3490-3240 Ma
- 1081 rocks of the Pilbara Supergroup, Pilbara Craton, Western Australia. Earth-Science
- 1082 Reviews 74, 197-240.

1083

- 1084 Van Kranendonk, M.J., Smithies, R.H., Hickman, A.H., Champion, D.C., 2007.
- 1085 Paleoarchean development of a continental nucleus: the East Pilbara Terrane of the
- 1086 Pilbara Craton. In Earth's oldest rocks, Van Kranendonk, M.J., Smithies, R.H.,
- 1087 Bennett, V.C. (Eds.): Elsevier, Amsterdam, The Netherlands. Developments in

1088 Precambrian Geology 15, 307-337.

- 1090 Wacey, D., 2009. Early Life on Earth, a Practical Guide. Topics in Geobiology 31
- 1091 (series editors: Landman, N.H., Harries, P.J.), Springer.

- 1093 Wacey, D., Kilburn, M.R., NcLoughlin, N., Parnell, J., Stoakes, C.A., Grovenor,
- 1094 C.R.M., Brasier M.D., 2008a. Use of NanoSIMS in the search for early life on Earth:
- ambient inclusion trails in a c. 3400 Ma sandstone. Journal of the Geological Society
- 1096 165, 43-53.
- 1097
- 1098 Wacey, D., Kilburn, M.R., Saunders, M., Cliff, J., Brasier, M.D., 2011. Microfossils
- 1099 of sulphur-metabolizing cells in 3.4-billion-year-old rocks of Western Australia.
- 1100 Nature Geoscience 4, 698-702.
- 1101
- 1102 Wacey, D., Saunders, M., Kong, C., Brasier, A.T., Brasier, M.D., 2015. 3.46 Ga Apex

1103 chert 'microfossils' reinterpreted as mineral artefacts produced during phyllosilicate

1104 exfoliation. Gondwana Research, doi:10.1016/j.gr.2015.07.010.

- 1105
- 1106 Walsh, M.M., 2004. Evaluation of Early Archean Volcaniclastic and volcanic Flow
- 1107 Rocks as Possible sites for Carbonaceous Fossil Microbes. Astrobiology 4, 29-437.
- 1108
- 1109 Walsh, M.M., Lowe, D.R., 1999. Modes of accumulation of carbonaceous matter in
- 1110 the Early Archaean: a petrographic and geochemical study of the carbonaceous cherts
- 1111 of the Swaziland Supergroup. In Geologic evolution of the Barberton Greenstone
- 1112 Belt, South Africa (ed. D. R. Lowe & G. R. Byerly) 329, 115–132. Boulder, CO:
- 1113 Geological Society of America. Special Paper.
- 1114
- 1115 Westall, F., de Ronde, C.E.J., Southam, G., Grassineau, N., Colas, M., Cockell, C.S.,
- 1116 Lammer, H., (2006). Implications of a 3.472-3.333 Gyr-old subaerial microbial mat

1117	from the Barberton	greenstone belt, South	n Africa for the UV	venvironmental
------	--------------------	------------------------	---------------------	----------------

- 1118 conditions on the early Earth Philosophical Transactions of The Royal Society B-
- 1119 Biological Sciences 361, 1857-1875.
- 1120
- 1121 Westall, F., Foucher, F., Cavalazzi, B., de Vries, S., Nijman, W., Pearson, V., Watson,
- 1122 J., Verchovsky, A., Wright, I., Rouzaud, J.-N., Marchesini, D., Anne, S., 2011.
- 1123 Volcaniclastic habitats for early life on Earth and Mars: a case study from ~3.5 Ga-
- 1124 old rocks from the Pilbara, Australia. Planetary and Space Science 59, 1093-1106.
- 1125
- 1126 Westall, F., Campbell, K.A., Bréhéret, J.G., Foucher, F., Gautret, P., Hubert, A.,
- 1127 Sorieul, S., Grassineau, N., Guido, D.M., 2015. Archean (3.33Ga microbe-sediment
- 1128 systems were diver and flourished in a hydrothermal context. Geology,
- 1129 doi:10.1130/G36646.1
- 1130
- 1131
- 1132 Figure Captions
- 1133

Figure 1. Location of the Chinaman Creek study area. a) Overview of the geology of
the East Pilbara Terrane, showing a series of domed granitoid complexes intruding
and overlain by volcano-sedimentary rocks of the Pilbara Supergroup. The Chinaman
Creek locality (red box) is found within the Marble Bar greenstone belt around 5 km
west of the town of Marble Bar. b) Geographical context of the East Pilbara Terrane
in Western Australia. Modified from Hickman (2008) and Brasier et al., 2011.

Figure 2. Field photograph looking southwest showing the south block of the 'Apex chert'. The stratiform chert (outlined in yellow) outcrops along the northwest-southeast trending ridge, while hydrothermal black chert veins (arrowed in red and labeled following the convention of Brasier et al., 2005, 2011) cut up through the underlying basalt often inter-fingering with (but not passing entirely through) the stratiform chert. Person for scale.

1147

1148 Figure 3. Geological map of the 'Apex chert' in the Chinaman Creek area. The area 1149 consists of three structural blocks, north, central, and south, defined by growth faults. 1150 The stratiform chert (unit 4 of Brasier et al., 2005, 2011) is the focus of this study and 1151 outcrops continuously in both the south and north blocks. Black chert veins cut up 1152 through the underlying basalt and underplate and interfinger with the strtaiform chert. 1153 The N1 vein houses the controversial 'microfossil' site of Schopf (1993). Locations of 1154 samples analysed in this study are numbered. Modified from Brasier et al. (2011). 1155 1156 Figure 4. Scans of geological thin sections, each accompanied by plane polarized 1157 light photomicrographs of sub-portions of the thin section, showing typical fabrics 1158 found within the stratiform 'Apex chert'. a-b) Silicified ash. c-d) Clotted

1159 carbonaceous chert. e-f) Banded microgranular chert (red and white arrows denote

alternating bands dominated by differing grain types), see also Supplementary Figures

1161 1 and 2. g-h) Metalliferous (Fe-rich) chert. i-j) Banded black-grey-white chert.

1162

Figure 5. Lobate fluffy grains from the stratiform chert. a-b) Typical lobate fluffy

1164 grains within microgranular chert with inclusions of wisps of chert and opaque

1165 crystals. Many large lobate grains (e.g., b) appear to be composites of multiple

smaller grains, consistent with an origin as carbon impregnated, clotted volcanic ash

1167 grains. c) Raman image from the edge of a fluffy grain showing its carbonaceous

1168 composition (red) and the quartz matrix (green). d) Typical Raman spectrum from a

1169 fluffy grain; note the well-developed carbon 'D' and 'G' peaks and small quartz peak.

1170

1171 Figure 6. Flake-like grains from the stratiform chert. a-b) Flake-like grains from the 1172 microgranular chert with accompanying Raman maps illustrating their carbonaceous 1173 (red) plus minor quartz (green) composition. Raman maps are from areas indicated by 1174 the yellow arrows and were constructed using the integrated intensities of the ~1600 1175 cm^{-1} carbon 'G' Raman band and the ~465 cm^{-1} guartz Raman band respectively. c) 1176 Elongate, curved, tapering flakes within microgranular chert. This is the dominant 1177 flake morphology in these cherts. d) Compressed lobate fluffy grains in silicified 1178 volcanic ash, with compression indicated by suturing of grains (arrows); their 1179 morphology superficially resembles flakes but their internal texture and chemistry 1180 distinguishes them from true flakes found in the microgranular chert. 1181

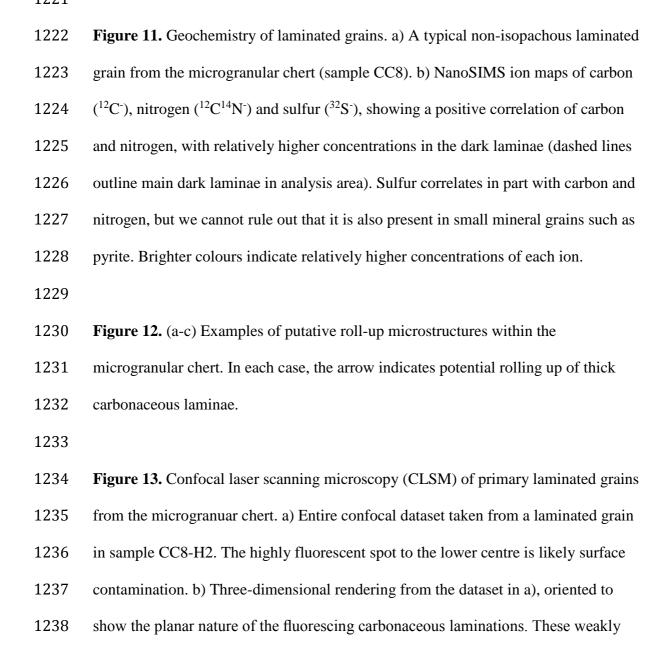
Figure 7. Primary laminated grains from the microgranular chert. a) Non-isopachous laminated microstructure in a region of otherwise fluffy lobate grains, interpreted as a reworked fragment of a larger laminated parent body. b-c) Non-isopachous, undulose and faintly crinkled laminated grains; note thickening of carbonaceous lamina at ridge crest (red arrow) and potential rolling up of upper thick carbonaceous lamina (yellow arrow). d) Thick carbonaceous band within a laminated grain composed of multiple finer carbonaceous laminae (arrow).

1190 Figure 8. Non-primary laminated grains from the stratiform chert. a-b) Silica 1191 intrusion into fluffy or flaky grains giving the impression of lamination. The silica 1192 'laminae' frequently do not traverse the whole grain and do not show the regular 1193 repeating pattern of primary lamination. The carbonaceous portions of the grain are 1194 often modified (e.g. pushed apart) by the intruding silica. c) Close up of a carbon-1195 silica boundary suggesting that carbonaceous material has been loosened by intruding 1196 silica (arrow), leading to a false gradation between layers. d) Microstructure that 1197 approximates tubular pumice, comprising isopachous laminae of tiny yellow-brown 1198 altered volcanic glass grains without carbon.

1199

1200 Figure 9. Mesoscale filament-like laminations in the stratiform chert. a) Scan of 1201 geological thin section (CC164) showing wrinkled, undulose laminae traversing the 1202 entire thin section (upper half of image) adjacent to a microgranular chert zone (lower 1203 portion of image). b) Plane polarized light image from the thin section shown in (a) 1204 showing dark filament-like laminae (e.g., dashed arrows), often stacked vertically into 1205 bundles several hundred micrometers thick. c) Image of the same thin section taken 1206 under crossed-polars showing quartz grains (e.g. arrows) entrained within some of the 1207 dark laminae. d) Higher magnification image from CC164 showing at least three 1208 quartz grains (solid arrows) entrained within filament-like laminae (dashed arrows), 1209 having their long axes parallel or at a shallow angle to the laminae. e) Particularly 1210 dense carbonaceous laminae within sample CCT23 wrapping around a number of 1211 quartz grains (examples arrowed). Again their long axes show similar alignment sub-1212 parallel to the trend of the laminae.

Figure 10. Mineralogy of laminated grains. a) A typical non-isopachous laminated grain from the microgranular chert (sample CC8). b) A two-colour overlay Raman map from area indicated in (a) showing the carbonaceous (red) and quartz (green) composition of the alternating bands. c) A typical Raman spectrum from a carbonaceous band illustrating the position and shapes of the carbon 'D' and 'G' peaks, plus small quartz peak. The carbon peak shapes are near identical to those from the fluffy and flaky grains (e.g., Fig. 5d).



undulate across the grain. c) Entire confocal dataset from a laminated grain in sample
CC8 displayed as a three-dimensional image, which again demonstrates a clear planar
character for the fluorescing carbonaceous laminae. d) Three-dimensional rendering
of the upper right portion of (c), highlighting the rolling up of laminae which
autofluoresce. These roll-ups (e.g., arrows) almost completely overturn reflexively;
roll-up is seen across at least seven of the upper laminae, and potentially in two
further lower laminae, thus is a common feature within this clast.

1246

1247 Figure 14. Chemistry of 'mesoscopic' laminations and entrained grains. a, c) Two 1248 examples of entrained, orientated grains within dark filament-like laminae from 1249 sample CCT23. b, d) Two colour overlay Raman maps from the areas indicated by the 1250 blue boxes in (a) and (c) respectively, showing the carbonaceous content of the dark 1251 laminae (red) and the quartz composition of the entrained grains (green). e) Typical 1252 Raman spectrum from the dark laminae, exhibiting near identical carbon 'D' and 'G' 1253 bands to those shown by other primary carbonaceous microstructures in this unit (e.g., 1254 Figs. 5d and 10c). The rather diffuse nature of the carbonaceous filaments is shown by 1255 the relatively strong Raman quartz bands indicating the filaments are now a mixture 1256 of carbon and silica.

1257

1259

1258 **Figure S1.** Textural characteristics of microclastic cherts at Chinaman Creek. a)

Microclastic chert (sample CC8) is unequivocally layered: in this scan of part of a thin

1260 section, alternating darker and lighter coloured bands can be observed, which indicate

1261 layers with a predominance of lobate fluffy ash clasts and elongate 'rip-up' flaky

1262 clasts, respectively. b) A second microclastic chert (sample CCT27) also consists of

1263 darker ash grains and lighter layers dominated by silica and flaky clasts, though here

1264	the banding is less distinct. There is a general coarsening-upward trend in grain size
1265	here. c) Microcrystalline and megaquartz veins regularly cut across thin sections but
1266	are rarely parallel to bedding. d) General texture of the microcrystalline cherts,
1267	showing a relatively well-sorted, clast-supported texture. Scale bar is 5 mm in (a) and
1268	(b) and 500 µm in (c) and (d).
1269	
1270	Figure S2. Variations of microclastic chert at Chinaman Creek. a) Slide scan of
1271	microclastic chert (sample CC43), which is rich in orientated pale clasts, some of
1272	which are banded. (b-c) Examples of banded clasts from sample CC43. Scale bar
1273	equals 3 mm in (a) and 500 µm in (b-c).
1274	
1275	Figure S3. Elemental analysis of the microclastic chert (sample CC8). a)
1276	Photomicrograph and elemental maps, showing enrichment of aluminium and
1277	potassium within a fluffy lobate clast, supporting an interpretation that this clast has a
1278	volcanic ash precursor. b) Photomicrograph and elemental maps (Al, C and O) from a
1279	flaky clast; this lacks enrichment in aluminium (or potassium, not shown) and
1280	possesses elevated levels of carbon.
1281	
1282	Movie S1. Reconstruction of carbonaceous laminated grains from confocal laser
1283	scanning microscopy data.